The Continuous Strength Method for the design of stainless steel hollow section columns

Itsaso Arrayago[a,*], Esther Real[a], Enrique Mirambell[a], Leroy Gardner[b]

[a]*Department of Civil and Environmental Engineering, Universitat Politècnica de Catalunya*

[b]*Department of Civil Engineering, Skempton Building, South Kensington Campus, Imperial College London*

*Corresponding author: Itsaso Arrayago. Jordi Girona 1-3, Building C1, 08034 Barcelona, Spain, itsaso.arrayago@upc.edu

ABSTRACT

The Continuous Strength Method (CSM) provides accurate resistance predictions for both stocky and slender stainless steel cross-sections; in the case of the former, allowance is made for the beneficial effects of strain hardening, while for the latter, design is simplified by the avoidance of effective width calculations. Although the CSM strain limits can be used in conjunction with advanced analysis for the stability design of members, for hand calculations, the method is currently limited to the determination of cross-sectional resistance only, i.e. member buckling resistance is not covered. To address this limitation, extension of the CSM to the design of stainless steel tubular section columns is presented herein. The proposed approach is based on the traditional Ayrton-Perry formulation, but features enhanced CSM cross-section resistances and a generalized imperfection parameter that is a function of cross-section slenderness. The value of the imperfection parameter increases as the slenderness of the cross-section reduces to compensate for the detrimental effect of plasticity on member stability that is not directly captured in the elastic/first yield Ayrton-Perry approach. The accuracy of the proposed approach is assessed against numerical results generated in the current study and existing experimental results collected from the literature. The presented comparisons show that the CSM provides consistently more accurate member buckling resistance predictions than the current EN 1993-1-4 design rules for all stainless steel grades. The reliability of the proposed approach is demonstrated through statistical analyses performed in accordance with EN 1990. Finally, the paper presents a framework through which the proposed approach can be developed for other cross-section types and materials.

KEYWORDS

Buckling; column; Continuous Strength Method; flexural buckling; SHS and RHS; stainless steel; structural design

HIGHLIGHTS

- A consistent CSM approach for the design of stainless steel members is presented.
- The new approach allows for the influence of material nonlinearity and strain hardening.
- The accuracy of the CSM for the design of columns is assessed against experimental and numerical data.
- The CSM provides consistently more accurate member buckling resistance predictions than current design rules.
- The reliability of the proposed approach is demonstrated through statistical analyses.

1. INTRODUCTION

The efficient design of structures is one of the mainstays of engineering practice, regardless of the considered construction material. This efficiency depends on the adopted structural form, but also on the accuracy of the provisions for the design of individual structural elements [1-3]. Given the high material cost of stainless steel in comparison to carbon steel, the development of efficient design expressions that fully exploit all the specific features of this corrosion-resistant material is particularly crucial.

The Continuous Strength Method (CSM) is a deformation-based design approach that provides a rational means of exploiting capacity gains arising from the spread of plasticity and strain hardening, allowing more efficient design of metallic structures. Currently, the method provides design expressions for calculating cross-sectional resistances under compression, bending and combined loading conditions. These rules can be used in conjunction with second order inelastic analysis with imperfections for the stability design of members [4,5], but design rules suitable for implementation by hand calculation for member buckling require further development. Several studies into the behaviour of stainless steel members subjected to combined loading [6,7] have highlighted the need for providing accurate flexural buckling and bending moment resistance predictions to act as suitable end points for design interaction curves. Hence, enhancing resistance predictions for members under isolated loading conditions will also lead to improvements under combined loading. Zhao et al. [7] proposed the use of

the CSM bending moment resistance as the bending end point in the design interaction equations for stainless steel beam-columns with stocky cross-sections, but no modification was proposed to the flexural buckling resistance (i.e. the compression end point). Previous efforts to extend the CSM to the design of stainless steel columns have been presented by Ahmed and Ashraf [8], though the method features several empirical-based modification factors to account for the nonlinear material response and further improvements are deemed possible. Other research accounting for strain hardening effects in stainless steel members, but based on the Direct Strength Method, can also be found [9,10].

A consistent new hand calculation approach for the design of stainless steel members subjected to compression, based on the CSM, that allows for the influence of material nonlinearity and strain hardening is presented in the current paper. The new proposals have a sound theoretical basis and are shown to provide more accurate predictions of the flexural buckling resistance of stainless steel columns than are achieved by current design codes. First, the current CSM provisions for cross-section resistance are described in Section 2. Secondly, existing experimental data and new finite element (FE) data on the capacity of stainless steel columns are assembled in Section 3. The theoretical development of the CSM for the prediction of member buckling resistance is then presented in Section 4, and the resulting formulations are assessed in Sections 5–7.

2. THE CONTINUOUS STRENGTH METHOD FOR CROSS-SECTION RESISTANCE

The Continuous Strength Method (CSM) is a deformation-based design approach that provides accurate predictions of the resistance of structural cross-sections composed of a range of metallic materials, including stainless steel [11,12], carbon steel [13,14] and aluminium [15]. The method was originally developed for stocky cross-sections and allowed the incorporation of strain hardening effects into the calculation of resistances. However, in recent research [16], the CSM has been extended to also cover slender cross-sections, dominated by local buckling effects. The method has been consistently shown to provide more accurate resistance predictions than traditional strength-based design rules, and has the additional benefit of providing explicit information on cross-section ductility, i.e. knowledge of the level of deformation required to reach the design capacity; this information is usually unknown. A further significant recent development is the implementation of the CSM within an advanced analysis framework [4,5,17].

The CSM is underpinned by a base curve that defines the maximum strain ε_{csm} that a cross-section can achieve prior to failure, evaluated in terms of its relative local slenderness $\bar{\lambda}_p$ and the yield strain ε_y, as shown in Eq. 1a and Eq. 1b for stocky and slender cross-sections, respectively, where ε_u is the ultimate material strain and C_1 is a material coefficient, both of which are described further below [11,12,16,18].

$$\frac{\varepsilon_{csm}}{\varepsilon_y} = \begin{cases} \frac{0.25}{\bar{\lambda}_p^{3.6}} \leq min\left(15, \frac{C_1\varepsilon_u}{\varepsilon_y}\right) for & \bar{\lambda}_p \leq 0.68 \\ \frac{1}{\bar{\lambda}_p^{1.05}}\left(1 - \frac{0.222}{\bar{\lambda}_p^{1.05}}\right) for & \bar{\lambda}_p > 0.68 \end{cases}$$

Eq. 1a

Eq. 1b

The local cross-sectional slenderness is calculated from Eq. 2, where σ_{cr} is the elastic local buckling stress of the full cross-section, and f_y is the 0.2% proof stress. The elastic buckling stress of the full cross-section can be determined using the simple analytical expressions set out in [19] or using numerical tools, e.g. CUFSM [20].

$$\bar{\lambda}_p = \sqrt{\frac{f_y}{\sigma_{cr}}} \quad \text{Eq. 2}$$

For stainless steel, the CSM utilises a bi-linear (elastic, linear hardening) material stress-strain model for ease of application in hand calculations developed for the austenitic and duplex stainless steel grades by Afshan and Gardner [11] and for the less ductile ferritic grades by Bock et al. [12]. The slope of the linear hardening region i.e. the strain hardening modulus E_{sh} is given by Eq. 3, in which f_u is the ultimate tensile strength of the material and ε_u is the ultimate strain that can be estimated from Eq. 4. The coefficients (C_1 to C_3) of the CSM material model are summarized in Table 1 for the different types of stainless steel.

$$E_{sh} = \frac{f_u - f_y}{C_2\varepsilon_u - \varepsilon_y} \quad \text{Eq. 3}$$

$$\varepsilon_u = C_3\left(1 - \frac{f_y}{f_u}\right) \quad \text{Eq. 4}$$

Once the maximum strain ε_{csm} that the cross-section can achieve has been calculated, the cross-section compression $N_{c,csm}$ and bending $M_{c,csm}$ resistances can be determined from Eqs. 5 and 6, respectively. In these equations, N_y is the squash (yield) load of the gross cross-section, M_{pl} and M_{el} are the plastic and

elastic bending moment capacities, W_{pl} and W_{el} are the plastic and elastic section moduli, respectively, α is a cross-section dependent exponent equal to 2 for tubular sections, and E is the Young's modulus.

$$N_{c,csm} = \begin{cases} N_y \left[1 + \frac{E_{sh}}{E} \left(\frac{\varepsilon_{csm}}{\varepsilon_y} - 1 \right) \right] & for \quad \bar{\lambda}_p \leq 0.68 \\ N_y \left(\frac{\varepsilon_{csm}}{\varepsilon_y} \right) & for \quad \bar{\lambda}_p > 0.68 \end{cases} \quad \text{Eq. 5}$$

$$M_{c,csm} = \begin{cases} M_{pl} \left[1 + \frac{E_{sh}}{E} \frac{W_{el}}{W_{pl}} \left(\frac{\varepsilon_{csm}}{\varepsilon_y} - 1 \right) - \left(1 - \frac{W_{el}}{W_{pl}} \right) \left(\frac{\varepsilon_{csm}}{\varepsilon_y} \right)^{-\alpha} \right] & for \quad \bar{\lambda}_p \leq 0.68 \\ M_{el} \left(\frac{\varepsilon_{csm}}{\varepsilon_y} \right) & for \quad \bar{\lambda}_p > 0.68 \end{cases} \quad \text{Eq. 6}$$

For cross-sections under combined compression plus bending, use of the EN 1993-1-1 [21] cross-section interaction curves, but anchored to the CSM end points, has been recommended and shown to provide accurate resistance predictions [22,23]. Note that although the cross-section interaction equations are the same for carbon steel and stainless steel, the member level beam-column interaction curves are different [24]. Having described the basis of the CSM cross-section design provisions in the current section, extension of the scope of the CSM to the prediction of member buckling resistance is presented in the remaining sections of this paper.

3. COLLECTION OF EXISTING EXPERIMENTAL DATA AND GENERATION OF NEW FE DATA

Existing experimental data on stainless steel square and rectangular hollow section (SHS and RHS) columns are assembled in this section. These data are complemented by further numerical results generated herein. Both groups of data are employed in Sections 5-7 to assess the accuracy and reliability of the new CSM member resistance functions derived in Section 4.

3.1 EXPERIMENTAL DATA COLLECTION

The behaviour of stainless steel SHS and RHS members subjected to compression has been extensively analysed through experimentation over the past few decades. The resulting test data on austenitic [25-30], ferritic [6,31,32] and duplex (or lean duplex) [33-36] stainless steel columns have been assembled herein, as summarized in Table 2. All collected data are used in the assessment of the CSM member

buckling design formulations presented in Section 4, while some of the data are used for the validation of the numerical models described in the present section.

3.2 FE MODEL VALIDATION

FE models of stainless steel columns were developed using the general-purpose software ABAQUS [37] and validated against the experimental results reported by Arrayago et al. [6]. The mid-surfaces of the cross-sections were modelled using four-noded shell elements with reduced integration, designated S4R [37]; these elements have been widely used in the modelling of cold-formed steel [38] and stainless steel [33,39] members. Computational efficiency and reliability of results was ensured by conducting a prior mesh convergence study, following which, a uniform mesh size of 5 mm was adopted. Local and global initial geometric imperfections were introduced into the FE model in the form of elastic buckling mode shapes obtained from prior linear buckling analyses; for the validation of the model, the measured imperfection amplitudes from the test specimens, as reported in [6], were introduced. The geometrically and materially nonlinear FE analyses were solved using the modified Riks method [37].

To replicate the pin-ended boundary conditions of the tests, the elements at the ends of the members were kinematically coupled and connected to two reference points. These reference points were positioned at a distance of 50 mm (corresponding to the knife-edge thickness) from the ends of the member, following the experimental setup [6]. At the lower reference point, all degrees of freedom except rotation around the minor axis were restrained; at the upper reference point, all degrees of freedom except longitudinal displacement and minor axis rotation were restrained. The load was then introduced as an imposed displacement at the upper reference point.

The measured material properties from the test specimens were incorporated into the FE models, considering separately the flat and corner regions of the cross-sections. The corner material properties, which are enhanced due to cold-working in the forming process, were applied to the curved regions of the cross-sections, but also extended into the adjacent flat regions by a distance equal to two times the thickness of the material, according to the recommendations in [40]. It was observed in [30,41] that coupons curve longitudinally when cut from cold-formed tubes, but return to their original straight shape when they are gripped and loaded in a tensile testing machine. During the straightening process, the bending residual stresses are approximately reintroduced; hence the obtained stress-strain curves

inherently include the influence of bending residual stresses, which do not therefore need to be explicitly incorporated into the FE models. Membrane residual stresses also exist in cold-formed stainless steel SHS and RHS, but are low in magnitude and have been shown to have a negligible influence on structural response [41,42]. Hence, membrane residual stresses have not been included in the developed FE models. The material parameters describing the stress-strain behaviour of the flat and corner regions of the modelled test specimens can be found in [6].

The experimental load-lateral deflection curves are compared to the corresponding FE curves in Figure 1, while the key results for the considered columns are reported in Table 3 as the mean values and the coefficients of variation (COV) of the numerical-to-experimental ratios of the ultimate loads and the corresponding lateral deflections, in which $N_{u,FE}$ and $N_{u,exp}$ are the FE and experimental ultimate axial loads, respectively, and $\delta_{u,FE}$ and $\delta_{u,exp}$ are the corresponding FE and experimental lateral displacements. These comparisons demonstrate that the presented numerical analysis approach is capable of accurately predicting the experimental ultimate loads and replicating the full experimental load-deformation histories. The FE failure modes are also in good agreement with the experimental results.

3.3 NUMERICAL PARAMETRIC STUDIES

Once the numerical model had been validated against the experimental results, a parametric study on a series of SHS and RHS stainless steel columns was carried out through a combination of Python and ABAQUS [37] tools. Considering that the measured initial imperfection amplitudes of the members tested in the experimental programme reported in [6] ranged between L/1000 and L/2000, where L is the member length, and that residual stresses are implicitly reflected in the FE models through the use of measured stress-strain properties [30,41], an imperfection amplitude of L/1500 was used in the parametric study. Eigenmode-affine local initial imperfections were also included in the FE models with amplitudes predicted using the Dawson and Walker model [43], as modified by Gardner and Nethercot [44].

The parametric study included austenitic, duplex and ferritic stainless steels, adopting the material properties obtained from the results reported in [6] for the ferritic grades and the material properties employed in a previous parametric study [7] for the austenitic and duplex alloys. The key material

parameters for the flat and corner regions of the cross-sections are presented in Table 4, where E is the Young's modulus, f_y is the proof stress corresponding to 0.2% plastic strain, f_u is the tensile strength, ε_u is the ultimate strain corresponding to f_u and n and m are strain hardening exponents. Finally, the full stress-strain curves were generated using the formulations presented in Arrayago et al. [45].

The minor axis flexural buckling behaviour of a variety of SHS and RHS stainless steel columns was investigated, utilising the general modelling assumptions described in the previous section. Four cross-sectional aspect ratios H/B equal to 1, 1.2, 1.5 and 2 were considered, with thicknesses ranging between 2 mm and 4 mm and member slendernesses $\bar{\lambda}$ ranging from 0.25-0.75.

4. DEVELOPMENT OF THE CSM FOR MEMBERS BUCKLING

The Continuous Strength Method (CSM) provides excellent resistance predictions for cross-sections, accounting for strain hardening effects in stocky sections and providing a direct and straightforward procedure to account for local buckling effects in slender sections. However, for hand calculations, the method is limited to cross-sectional resistance predictions in its current form; extension of the CSM to also cover member buckling is undertaken herein.

The behaviour of slender stainless steel columns is dominated by member instability, with failure occurring at low average stress levels, below the 0.2% proof stress, or even below the proportional limit, of the material. However, for columns of low to intermediate slenderness, the average axial stress at failure can exceed the 0.2% proof stress, as the member is sufficiently stocky to maintain stability even after partial plastification of the critical cross-section. The resistance of these columns is therefore generally underestimated by current design specifications in which the maximum attainable stress is limited to the 0.2% proof stress. Accounting for strain hardening effects, a new CSM-based approach is proposed herein for stainless steel SHS and RHS columns.

4.1 FLEXURAL BUCKLING DESIGN PROVISIONS IN CURRENT STANDARDS

Traditional design provisions for stainless steel columns given in current standards, such as EN 1993-1-4 [1] and AS/NZS4673 [2], are based on the Ayrton-Perry buckling formulation [46] utilised in EN 1993-1-1 [21] for carbon steel members, where the design column strength $N_{b,Rd}$ is determined by reducing the characteristic cross-section squash load $N_{c,Rk} = Af_y$, where A is the cross-section area (or

effective area for Class 4 sections) and f_y is the 0.2% proof stress, to account for flexural buckling effects through the buckling reduction factor χ, as given in Eq. 7, in which γ_{M1} is the partial factor for member instability.

$$N_{b,Rd} = \frac{\chi N_{c,Rk}}{\gamma_{M1}} \quad \text{Eq. 7}$$

The reduction factor χ is calculated from the corresponding buckling curve, as given in Eqs. 8 and 9, as a function of the member slenderness $\bar{\lambda} = \sqrt{N_{c,Rk}/N_{cr}}$, where N_{cr} is the elastic buckling load of the member.

$$\chi = \frac{1}{\phi + \sqrt{\phi^2 - \bar{\lambda}^2}}, \text{ but } \leq 1 \quad \text{Eq. 8}$$

$$\phi = 0.5\left[1 + \eta + \bar{\lambda}^2\right] \quad \text{Eq. 9}$$

In EN 1993-1-4 [1], the imperfection parameter η is given by $\eta = \alpha_{EN}\left(\bar{\lambda} - \bar{\lambda}_0\right)$, with $\alpha_{EN} = 0.49$ and $\bar{\lambda}_0 = 0.4$ for cold-formed hollow sections, while AS/NZS4673 [2] utilises a nonlinear generalized imperfection factor and provides different buckling curves for different stainless steel grades. AS/NZS4673 [2] also allows the use of a tangent modulus approach in the prediction of flexural buckling resistance, where the nonlinear stress-strain response of the material is directly considered, though the design procedure is iterative.

Recent reliability analyses carried out by Afshan et al. [47] in accordance with EN 1990 [48] indicated that the flexural buckling curve currently specified in EN 1993-1-4 [1] for cold-formed stainless steel SHS and RHS columns yielded a required partial safety factor γ_{M1} that exceeded the recommended value of 1.10, suggesting that a lower buckling curve is required. It was also proposed that different buckling curves are necessary for different stainless steel grades to reflect their varying degrees of material nonlinearity. The revised buckling curves have already been included in the Fourth Edition of the Design Manual for Structural Stainless Steel [18] and are due to be incorporated into the upcoming version of EN 1993-1-4; these curves are therefore considered in the comparisons made in the present paper. The proposed revised curves are similar to buckling curve *c* [1,21], adopting the same imperfection factor $\alpha_{EN} = 0.49$ for all stainless steels, but with different limiting slendernesses of $\bar{\lambda}_0 = 0.3$ for austenitic and duplex and $\bar{\lambda}_0 = 0.2$ for ferritic stainless steel alloys.

4.2 DERIVATION OF THE CSM FORMULAE FOR MEMBER BUCKLING

4.2.1 INTRODUCTION

Derivation of the CSM design formula for member buckling is based on consideration of a pin-ended column with a half sine-wave initial geometrical imperfection of magnitude e_0, subjected to an axial compressive load. From the classical elastic flexural equilibrium equation of the imperfect column Trahair et al. [49], the most heavily loaded cross-section reaches first yield at an applied load level $N_{b,Rk}$ given by Eq. 10.

$$\frac{N_{b,Rk}}{N_{c,Rk}} + \frac{1}{\left(1 - \frac{N_{b,Rk}}{N_{cr}}\right)} \frac{N_{b,Rk} e_0}{M_{el}} = 1 \qquad \text{Eq. 10}$$

where M_{el} is the elastic bending moment resistance of the cross-section and N_{cr} is the elastic critical buckling load of the member. In Eurocode 3, the above expression is presented through Eqs. 7 to 9 where, based on the first yield failure criterion, the generalized imperfection factor $\eta = \frac{e_0 A}{W_{el}}$ is adopted. When the slenderness plateau $\bar{\lambda}_0$ is introduced, the generalized imperfection factor can be expressed as per Eq. 11. This first yield failure criterion, or slight modification thereof, has traditionally been used for the development of column buckling rules in Europe, but does not represent well the nonlinear material response of stainless steel [50,51].

$$\eta = \alpha_{EN}\left(\bar{\lambda} - \bar{\lambda}_0\right) \qquad \text{Eq. 11}$$

4.2.2 OUTLINE OF THE METHOD

To reflect the particular characteristics of stainless steel, the elastic cross-sectional resistances in compression $N_{c,Rk} = Af_y$ and bending $M_{el} = W_{el} f_y$ used in Eq. 10 can be replaced by the corresponding CSM resistances defined in Eqs. 5 and 6 to give Eq. 12, where $N_{c,csm,Rk}$ and $M_{c,csm,Rk}$ are the CSM cross-section compression and bending moment resistances and $N_{b,csm,Rk}$ is the flexural buckling resistance of the column according to the CSM. It is of course recognized that in order to reach the CSM cross-section resistances in the stocky range, material nonlinearity will be experienced, and the traditional elastic/first yield assumption of the Ayrton-Perry formulation no longer holds. This is

considered through the definition of the CSM equivalent imperfection amplitude $e_{0,csm}$, as discussed in the following sections.

$$\frac{N_{b,csm,Rk}}{N_{c,csm,Rk}} + \frac{1}{\left(1 - \frac{N_{b,csm,Rk}}{N_{cr}}\right)} \frac{N_{b,csm,Rk} e_{0,csm}}{M_{c,csm,Rk}} = 1 \quad \text{Eq. 12}$$

Defining $\sigma_{b,csm} = N_{b,csm,Rk}/A$, $\sigma_{c,csm} = N_{c,csm,Rk}/A$ and $\sigma_{cr} = N_{cr}/A$, Eq. 12 can be re-written in terms of stresses, to give Eq. 13. Note that $\sigma_{c,csm}$ and $\sigma_{b,csm}$ refer to the failure stress of the cross-section and member (due to flexural buckling), respectively.

$$\frac{\sigma_{b,csm}}{\sigma_{c,csm}} + \frac{1}{\left(1 - \frac{\sigma_{b,csm}}{\sigma_{cr}}\right)} \frac{\sigma_{b,csm} e_{0,csm}}{\frac{M_{c,csm}}{A}} = 1 \quad \text{Eq. 13}$$

Eq. 13 can be rewritten as Eq. 14, where η_{csm} is a new generalised imperfection factor given by Eq. 15.

$$\left(\sigma_{c,csm} - \sigma_{b,csm}\right)\left(\sigma_{cr} - \sigma_{b,csm}\right) = \sigma_{b,csm}\sigma_{cr}\eta_{csm} \quad \text{Eq. 14}$$

$$\eta_{csm} = \frac{e_{0,csm} A}{M_{c,csm,Rk}/\sigma_{c,csm}} = e_{0,csm} \frac{N_{c,csm,Rk}}{M_{c,csm,Rk}} \quad \text{Eq. 15}$$

Presenting Eqs. 12 and 13 in the familiar format of Eurocode 3, the CSM flexural buckling resistance is given by Eq. 16, while the corresponding member slenderness $\bar{\lambda}_{csm}$ and the buckling reduction factor χ_{csm} are given by Eq. 17 and Eqs. 18 and 19, respectively.

$$N_{b,csm,Rd} = \frac{\chi_{csm} N_{c,csm,Rk}}{\gamma_{M1}} \quad \text{Eq. 16}$$

$$\bar{\lambda}_{csm} = \sqrt{N_{c,csm,Rk}/N_{cr}} \quad \text{Eq. 17}$$

$$\chi_{csm} = \frac{1}{\phi_{csm} + \sqrt{\phi_{csm}^2 - \bar{\lambda}_{csm}^2}} \quad \text{Eq. 18}$$

$$\phi_{csm} = 0.5\left[1 + \eta_{csm} + \bar{\lambda}_{csm}^2\right] \quad \text{Eq. 19}$$

The proposed CSM approach for the flexural buckling resistance of stainless steel columns given by Eqs. 16 to 19 is equivalent to the procedure described in Section 4.1 and adopted in current standards [1-2,21] but requires the definition of a new generalised imperfection factor η_{csm}, given in Eq. 15, in which $e_{0,csm}$ is the CSM equivalent imperfection amplitude. From Eq. 15, introducing the slenderness plateau $\bar{\lambda}_0$ and the relationships $\lambda = L/i$, $i^2 = I/A$ and $W_{el} = I/v$, the new generalized imperfection

factor η_{csm} can be expressed as in Eq. 20. In these relationships, *L* is the length of the column, *I* is the relevant second moment of area, *A* is the gross-section area and *v* is the distance from neutral axis to the extreme fibre.

$$\eta_{csm} = \frac{e_{0,csm}\pi}{L\left(\frac{i}{v}\right)}\sqrt{\frac{E}{\sigma_{c,csm}}}\left(\bar{\lambda}_{csm} - \bar{\lambda}_0\right)\frac{\sigma_{c,csm}W_{el}}{M_{c,csm,Rk}} = \alpha_{csm}\left(\bar{\lambda}_{csm} - \bar{\lambda}_0\right) \quad \text{Eq. 20}$$

The CSM equivalent imperfection amplitude is obtained from Eqs. 20 and 15 as:

$$e_{0,csm} = \alpha_{csm}\left(\bar{\lambda}_{csm} - \bar{\lambda}_0\right)\frac{M_{c,csm,Rk}}{N_{c,csm,Rk}} \quad \text{Eq. 21}$$

This expression is similar to the imperfection factor given in Section 7 of EN 1993-1-1 [21] for the calculation of the unique (back-calculated) imperfection amplitude $e_{0,el,EN}$ to be adopted with a linear elastic cross-section check in the design of carbon steel columns by second order elastic analysis, as given by Eq. 22. From Eqs. 20 and 11, the relationship between α_{csm} and α_{EN} can be obtained, as shown in Eq. 23, in which $N_{pl} = Af_y$.

$$e_{0,el,EN} = \alpha_{EN}\left(\bar{\lambda}_{csm} - \bar{\lambda}_0\right)\frac{M_{el}}{N_{pl}} \quad \text{Eq. 22}$$

$$\alpha_{csm} = \alpha_{EN}\frac{e_{0,csm}}{e_{0,el,EN}}\sqrt{\frac{f_y}{\sigma_{c,csm}}}\frac{\sigma_{c,csm}W_{el}}{M_{c,csm,Rk}} = \alpha_{EN}\frac{e_{0,csm}}{e_{0,el,EN}}\sqrt{\frac{f_y}{\sigma_{c,csm}}}\frac{N_{c,csm,Rk}M_{el}}{M_{c,csm,Rk}N_{pl}} \quad \text{Eq. 23}$$

Figure 2 presents the back-calculated equivalent bow imperfection amplitudes e_0 for the design of columns by second order elastic analysis using different linear cross-section interaction equations – elastic, plastic and CSM-plastic–, with the corresponding end points indicated. Critical cross-section *N*-*M* equilibrium paths obtained by second order elastic analysis (GNIA) are plotted along with these interaction diagrams in the figure, where *N* is the applied axial compression and *M* is the corresponding second order bending moment in the case of the appropriate bow imperfection amplitude e_0, calculated from $M = (Ne_0)/(1 - N/N_{cr})$. The intersection point of the different equilibrium paths with their corresponding interaction diagrams provides the load level (as marked with the horizontal line) corresponding to the buckling resistance of the column. The back-calculated imperfection amplitudes are higher when the linear plastic curve is considered, in line with the imperfection amplitudes given in

Table 7.1 of [21] for the reference relative bow imperfections, and Eq. 22 in the case that M_{el} is replaced by M_{pl} [51].

As shown in Figure 2, the equivalent imperfection amplitude $e_{0,csm}$ required for use in conjunction with the linear CSM-plastic interaction is higher again. Determination of this CSM equivalent imperfection amplitude, which is utilized in the definition of the CSM imperfection factor α_{csm}, is addressed in the following section for stainless steel SHS and RHS columns.

4.2.3 CSM EQUIVALENT IMPERFECTION AMPLITUDE $e_{0,csm}$ AND IMPERFECTION FACTOR α_{csm}

For the definition of the CSM imperfection factor α_{csm} it is necessary to analyse the required equivalent CSM column imperfection amplitudes $e_{0,csm}$ for stainless steel columns of different proportions and material grades. Critical cross-section *N-M* equilibrium paths and interaction diagrams are shown in Figures 3 to 5 for some typical SHS/RHS columns in austenitic, ferritic and duplex stainless steel, respectively. For each stainless steel grade, two members, with stocky cross-sections ($\bar{\lambda}_p \approx 0.35$) and two different lengths (giving member slenderness values around 0.75 and 1.25) are considered. For each cross-section, three linear interaction diagrams with different end points are plotted in Figures 3 to 5: (i) based on first yield using N_{pl} and M_{el}, (ii) based on N_{pl} and M_{pl} and (iii) considering the CSM axial and bending cross-section resistances, $N_{c,csm}$ and $M_{c,csm}$. Second order elastic analysis (GNIA) paths corresponding to the back-calculated bow imperfection amplitudes for the numerically predicted resistances $N_{b,FE}$ are also included in these figures. The back-calculated imperfections have been determined such that the intersection between the GNIA paths and the different interaction diagrams occur at the numerically predicted buckling resistances of the columns $N_{b,FE}$, as obtained from GMNIA; these resistances are indicated with horizontal lines in Figures 3 to 5.

It is important to note that the required bow imperfection amplitudes increase with decreasing cross-sectional slenderness, since plasticity effects, which are ignored in GNIA but have to be compensated for by the use of a larger imperfection, become more relevant. The same approach is used in the EN 1993-1-1 provisions for member design by second order elastic analysis, in which a larger equivalent bow imperfection is used when a plastic rather than an elastic axial-moment cross-section interaction curve is used [51]. This is illustrated in Figure 6, where normalized plastic-CSM interaction diagrams

are shown for different cross-section slenderness values. As $\bar{\lambda}_p$ values increase, the plastic-CSM interaction diagrams tend towards the elastic interaction diagram corresponding to the column buckling design approaches adopted in current Standards [1-2,21]. Thus, it is necessary to determine appropriate imperfection amplitudes for use with linear interaction diagrams using CSM cross-section resistances as the end points (Eq. 12), as a function of the local slenderness of the cross-sections.

For the determination of the required CSM bow imperfection amplitude $e_{0,csm}$, the available experimental and numerical column buckling resistance data described in Section 3 have been employed. The required equivalent experimental (or numerical) imperfection amplitudes $e_{0,el,EN}$ and $e_{0,csm}$ can be back-calculated by setting $N_{b,Rk}$ and $N_{b,csm,Rk}$ in Eqs. 10 and 12, equal to the experimental or numerical column resistances. Then, the $e_{0,csm}/e_{0,el,EN}$ ratios can be calculated and plotted against the corresponding local slenderness $\bar{\lambda}_p$, as per Figure 7, for the different stainless steel grades considered in the analysis. In this analysis, and throughout the paper, local slenderness values have been obtained using elastic local buckling stresses derived from eigenvalue analyses, though the simplified analytical expressions provided in [19] yield very similar results. From Figure 7, a clear descending trend in $e_{0,csm}/e_{0,el,EN}$ can be observed with increasing $\bar{\lambda}_p$ values for the three materials.

The relationship between $e_{0,csm}/e_{0,el,EN}$ and $\bar{\lambda}_p$ is defined by Eq. 24, where the required values of the coefficients C_5 and C_6 are provided in Eqs. 25 and 26. These coefficients have been defined in such a way that they account for the different stress-strain characteristics of the different stainless steel grades through their dependency on f_u/f_y. As shown in Figure 7, the proposed linear relationship (Eq. 24) and coefficients C_5 and C_6 provide a good fit to the $e_{0,csm}/e_{0,el,EN}$ results back-calculated from experimental and numerical column buckling resistances. Note that, at the CSM limiting local slenderness $\bar{\lambda}_p = 0.68$, the $e_{0,csm}/e_{0,el,EN}$ ratio is equal to 1.0, i.e. the CSM and EN equivalent imperfection amplitudes converge. This is to be expected because at $\bar{\lambda}_p = 0.68$, the CSM cross-section resistances ($N_{c,csm}$ and $M_{c,csm}$) are equal to N_{pl} and M_{el}. Beyond this slenderness limit (i.e. for all slender sections), a constant value of to 1.0 is adopted for the $e_{0,csm}/e_{0,el,EN}$ ratio.

$$\frac{e_{0,csm}}{e_{0,el,EN}} = \begin{cases} C_5 - C_6\bar{\lambda}_p & for \quad \bar{\lambda}_p \leq 0.68 \\ 1 & for \quad \bar{\lambda}_p > 0.68 \end{cases} \qquad \text{Eq. 24}$$

$$C_5 = 1 + 0.68C_6 \quad \text{Eq. 25}$$

$$C_6 = 1.2(f_u/f_y) \quad \text{Eq. 26}$$

4.2.4 COLUMNS WITH SLENDER CROSS-SECTIONS

The prediction of the flexural buckling resistance of columns with slender cross-sections (i.e. $\bar{\lambda}_p > 0.68$) needs to account for cross-section resistance reductions due to premature local buckling as opposed to cross-section resistance gains due to strain hardening. These reductions can be considered through the CSM strength curve for slender sections –see Eq. 1b–, or indeed using the traditional effective width method. The first approach is more direct, simpler and based on gross-sectional properties. Since for cross-sections with $\bar{\lambda}_p > 0.68$, $e_{0,csm}/e_{0,el,EN} = 1$, $\sigma_{c,csm} = f_y$ and $\sqrt{\frac{f_y}{\sigma_{c,csm}}\frac{N_{c,csm,Rk}M_{el}}{M_{c,csm,Rk}N_{pl}}} = 1$, Eq. 23 becomes $\alpha_{csm} = \alpha_{EN}$, and thus the CSM approach is similar to the currently codified method, with the only difference being the way in which local buckling is treated based on the full cross-section slenderness [19] and Eq. 1b for the CSM and based on the plate-by-plate effective width method for EN 1993-1-4 [1].

4.2.5 ILLUSTRATIVE CSM BUCKLING CURVES

With the aim of illustrating the proposed CSM member design approach, typical $N_{b,csm}/N_{pl}$ curves are calculated for different materials and cross-section slenderness values $\bar{\lambda}_p$ and plotted in Figures 8 to 10. Note that the specific $N_{b,csm}/N_{pl}$ curve for a given member will depend on its particular geometrical and material parameters; thus, the curves shown in the figures only represent the CSM buckling curves for specific cases. Austenitic, ferritic and duplex stainless steel SHS/RHS columns are considered in Figures 8 to 10, respectively, considering four different cross-section slenderness values. Buckling curve *c*, provided in [18] for stainless steel hollow sections, is also shown for comparison. It is evident from Figures 8 to 10 that, for a given material, the highest buckling curves are obtained for those cross-sections with the lowest local slenderness $\bar{\lambda}_p$. In addition, it can be observed that the obtained buckling curves are higher for those materials in which strain hardening effects are more significant i.e. the austenitic stainless steel buckling curves are higher than the duplex and ferritic buckling curves.

In a similar manner to Figures 8 to 10, Figures 11 to 13 show the increase (or decrease) in column buckling resistance obtained using the CSM approach over the Eurocode approach for the considered austenitic, ferritic and duplex stainless steel columns; the data are grouped into four bands by cross-section slenderness value. From these figures it is evident that the largest benefit is obtained for members with both low column and cross-section slenderness.

5. ASSESSMENT OF THE CSM APPROACH FOR COLUMNS WITH STOCKY CROSS-SECTIONS

An assessment of the proposed CSM approach for the stability design of stainless steel columns is presented in this section by comparing the predicted flexural buckling resistances with the experimental and numerical results introduced in Section 3. Note that although the proposed approach is applicable to a number of materials and cross-section shapes for which the CSM has been developed, this paper only covers the assessment of SHS and RHS members, which are the most commonly used stainless steel cross-sections. The assessment is presented separately for columns with stocky and slender cross-sections. In this section, members with cross-section slenderness values $\bar{\lambda}_p \leq 0.68$ are considered to evaluate the beneficial influence of strain hardening, which is not included in the Eurocode 3 buckling curves. Note that, for the presented comparisons, the EN 1993-1-4 buckling curves are taken as those developed in [47], which have already been included in the Design Manual [18] and are due to be incorporated into the upcoming revision to EN 1993-1-4.

Tables 5 and 6 present the mean and COV values of the predicted-to-experimental (or FE) ratios for the considered flexural buckling design approaches for different data subsets. To illustrate more clearly the improvements achieved using the proposed CSM approach, results corresponding to the stockiest cross-sections ($\bar{\lambda}_p \leq 0.5$) are presented in Table 5, separated by stocky ($\bar{\lambda}_{csm} \leq 1$) and slender ($\bar{\lambda}_{csm} > 1$) members, while Table 6 shows results for the full cross-section slenderness range. In the tables, N_u is the ultimate test or FE resistance, $N_{b,EN}$ is the resistance obtained using the revised Eurocode buckling curves [18,47] and $N_{b,csm}$ is the resistance obtained using the CSM. In the presented assessment, cross-section slenderness values have been calculated using Eq. 2, in which the elastic local buckling stress under pure compression σ_{cri} was obtained using CUFSM [20].

The results presented in Tables 5 and 6 show that the proposed CSM approach provides improved predictions of the resistance of stainless steel SHS and RHS columns since higher predicted-to-test/FE resistance ratios $N_{b,pred}/N_u$, with lower or similar scatter, are obtained. The results reported in Table 5 show a greater improvement in the prediction of the ultimate capacity of columns with stocky cross-sections for duplex stainless steel than for austenitic grades, despite the lesser degree of strain hardening. This is because the proportion of data in the lowest cross-section slenderness range $\bar{\lambda}_p \leq 0.4$, in which greater improvements are expected, is higher for the duplex stainless steel database than for the austenitic stainless steel database, as shown in Figures 11 and 13. Figure 14 presents similar results by plotting the predicted-to-experimental (or FE) resistance ratios against the corresponding member slenderness (see Figure 14(a)) and cross-sectional slenderness (see Figure 14(b)) for the developed method and the revised Eurocode 3 flexural buckling curves provided in [18]. From these figures it can be also seen that the prediction of column buckling resistances is improved when the proposed CSM method is adopted.

6. ASSESSMENT OF THE CSM APPROACH FOR COLUMNS WITH SLENDER CROSS-SECTIONS

In this section, an assessment of the CSM approach for the design of stainless steel members with slender cross-sections (i.e. $\bar{\lambda}_p > 0.68$) is presented. As in the previous section, the revised Eurocode 3 buckling curves [18,47] are considered throughout the comparisons. The results calculated using the CSM and EN 1993-1-4 [1], utilising the effective width expressions developed in [53] and adopted in [1,18], are compared with the test and FE results in Table 7. It is evident from the comparisons that the CSM and EN 1993-1-4 yield very similar results when applied to stainless steel SHS/RHS columns with slender cross-sections. The CSM is however simpler to use, since no effective width calculations are required, yet a similar level of accuracy is achieved; this is therefore considered to be an overall improvement. Similar conclusions can be drawn from Figure 15, where the predicted-to-experimental (or FE) ratios are plotted against member slenderness (see Figure 15(a)) and against cross-sectional slenderness (see Figure 15(b)).

7. RELIABILITY ANALYSIS

The reliability of the proposed CSM and Eurocode 3 [18,47] member design approaches is assessed in this section. The statistical analyses have been carried out according to EN 1990, Annex D [48], while the statistical parameters corresponding to the material and geometrical variations of the different stainless steel grades have been extracted from Afshan et al. [54]. The considered material overstrength ratios are 1.3 for austenitic, 1.2 for ferritic and 1.1 for duplex stainless steel, with COV values equal to 0.060, 0.045 and 0.030 respectively, and the COV of the geometric properties was taken as 0.050.

A summary of the most relevant statistical parameters is presented in Table 8. In this table, b is mean value of the correction factor, V_δ is the coefficient of variation of the errors relative to the experimental results, V_r is the combined coefficient of variation and γ_{M1} is the calculated required partial safety factor. Note that for the calculation of the parameter b, which represents the mean value of the correction factor, the adopted approach is slightly different from that stated in [48], since for this method the relative weight of specimens with high ultimate load in the determination of b is higher than for specimens failing at lower loads, meaning that the value of b is biased towards data with high absolute resistances. The adopted b values have been calculated herein following the approach described in [55,56], with $b = \frac{1}{n}\sum_{i=1}^{n}\frac{N_{u,i}}{N_{b,pred,i}}$, where n is the number of considered specimens, N_u the is the experimental (or FE) ultimate resistance and $N_{b,pred}$ is the predicted column resistance.

According to the results gathered in Table 8, the proposed CSM design approach for stainless steel columns can be safely applied to members with both stocky and slender cross-sections, and to the different stainless steel grades considered, since the calculated required γ_{M1} values lie below the partial safety factor γ_{M1} currently recommended in EN 1993-1-4 [1], which is equal to 1.10.

8. SUMMARY OF CSM MEMBER BUCKLING DESIGN PROPOSALS

Based on the described analyses, the proposed CSM design formulae for member buckling are summarised as follows:

$$N_{b,csm,Rd} = \frac{\chi_{csm} N_{csm,Rk}}{\gamma_{M1}} \qquad \text{Eq. 16}$$

$$\chi_{csm} = \frac{1}{\phi_{csm} + \sqrt{\phi_{csm}^2 - \bar{\lambda}_{csm}^2}} \quad \text{Eq. 18}$$

$$\phi_{csm} = 0.5\left[1 + \alpha_{csm}\left(\bar{\lambda}_{csm} - \bar{\lambda}_0\right) + \bar{\lambda}_{csm}^2\right] \quad \text{Eq. 19}$$

$$\bar{\lambda}_{csm} = \sqrt{N_{csm,Rk}/N_{cr}} \quad \text{Eq. 17}$$

$$\alpha_{csm} = \alpha_{EN} \frac{e_{0,csm}}{e_{0,el,EN}} \sqrt{\frac{f_y}{\sigma_{c,csm}}} \frac{N_{c,csm,Rk} M_{el}}{M_{c,csm,Rk} N_{pl}} \quad \text{Eq. 23}$$

$$\frac{e_{0,csm}}{e_{0,el,EN}} = \begin{cases} C_5 - C_6 \bar{\lambda}_p & for \quad \bar{\lambda}_p \leq 0.68 \\ 1 & for \quad \bar{\lambda}_p > 0.68 \end{cases} \quad \text{Eq. 24}$$

$$C_5 = 1 + 0.68 C_6 \quad \text{Eq. 25}$$

$$C_6 = 1.2\left(f_u / f_y\right) \quad \text{Eq. 26}$$

with α_{EN} being the EN 1993-1-4 imperfection factor.

9. CONCLUSIONS

A new design approach for determining the flexural buckling resistance of stainless steel columns based on the Continuous Strength Method (CSM) has been presented. Previously, since the CSM only covered cross-section resistance, assessment of member stability (within the CSM framework) was only possible in conjunction with second order inelastic analysis [4,5,17]. The new approach presented in this paper extends the CSM to member buckling, allowing for consideration of strain hardening and local buckling effects for stainless steel SHS and RHS columns. The proposed approach builds on the traditional Ayrton-Perry based design formulation, but considers a different generalized imperfection parameter that depends on the cross-sectional slenderness and considered material, introducing strain hardening effects directly into the formulation. The value of the imperfection parameter increases as the slenderness of the cross-section reduces to compensate for the detrimental effect of plasticity on member stability that is not directly captured in the elastic/first yield Ayrton-Perry approach. An assessment of the CSM and Eurocode 3 column buckling design approaches against experimental and numerical results showed that the proposed CSM provides improved predictions of the resistance of SHS and RHS columns with stocky cross-sections. For columns with slender cross-sections, the CSM

provided similar results to Eurocode 3, using the effective width method, but is simpler to apply. The reliability of the proposed approach was demonstrated through statistical analyses.

The proposed new CSM approach provides a framework that can be extended to further cross-section types and materials, as well as to other failure modes, such as lateral-torsional buckling and loading conditions, such as axial load plus bending.

ACKNOWLEDGEMENTS

The authors acknowledge the funding from MINECO (Spain) under Project BIA2016-75678-R, AEI/FEDER, UE "Comportamiento estructural de pórticos de acero inoxidable. Seguridad frente a acciones accidentales de sismo y fuego". The first author would also like to acknowledge the financial support provided by the Spanish Ministerio de Educación, Cultura y Deporte through the José Castillejo-2018 scholarship.

REFERENCES

[1] EN 1993-1-4:2006+A1:2015. Eurocode 3: Design of Steel Structures – Part 1-4: General Rules. Supplementary Rules for Stainless Steels, including amendment A1 (2015). Brussels, European Committee for Standardization (CEN), 2015.

[2] Australian/New Zealand Standard. Cold-formed stainless steel structures. AS/NZS 4673:2001, Sydney, Australia, 2001.

[3] Specification for the Design of Cold-Formed Stainless Steel Structural Members. ASCE Standard SEI/ASCE 8-02, Reston, VA, American Society of Civil Engineers, 2002.

[4] Fieber A., Gardner L. and Macorini L. Design of structural steel members by advanced inelastic analysis with strain limits. *Engineering Structures*. 199, 109624, 2019.

[5] Fieber A., Gardner L. and Macorini L. Structural steel design using second-order inelastic analysis with strain limits. *Journal of Constructional Steel Research*, 168, 105980, 2020.

[6] Arrayago I., Real E. and Mirambell E. Experimental study on ferritic stainless steel RHS and SHS beam-columns. *Thin-Walled Structures*, 100, 93–104, 2016.

[7] Zhao O., Gardner L. and Young B. Behaviour and design of stainless steel SHS and RHS beam-columns, *Journal of Constructional Steel Research*, 106, 330–345, 2016.

[8] Ahmed S., Ashraf M., Anwar-Us-Saadat M. The Continuous Strength Method for slender stainless steel cross-sections. *Thin-Walled Structures*, 107, 362–376, 2016.

[9] Arrayago I., Rasmussen K.J.R. and Real E. Full slenderness range DSM approach for stainless steel hollow cross-sections. *Journal of Constructional Steel Research*, 133, 156–166, 2017.

[10] Arrayago I., Rasmussen K.J.R. and Real E. Full slenderness range DSM approach for stainless steel hollow cross-section columns and beam-columns. *Journal of Constructional Steel Research*, 138, 246–263, 2017.

[11] Afshan S. and Gardner L. The continuous strength method for structural stainless steel design. *Thin-Walled Structures*, 68, 42–49, 2013.

[12] Bock M., Gardner L. and Real E. Material and local buckling response of cold-formed ferritic stainless steel sections. *Thin-Walled Structures*, 89, 131–141, 2015.

[13] Yun X. and Gardner L. The continuous strength method for the design of cold-formed steel non-slender tubular cross-sections. *Engineering Structures*, 175, 549–564, 2018.

[14] Gardner L., Wang F. and Liew A. Influence of strain hardening on the behavior and design of steel structures. *International Journal of Structural Stability and Dynamics*, 11(5), 855-875, 2011.

[15] Su M., Young B. and Gardner L. The continuous strength method for the design of aluminium alloy structural elements. Engineering Structures, 122, 338–348, 2016.

[16] Zhao O., Afshan S. and Gardner L. Structural response and continuous strength method design of slender stainless steel cross-sections. *Engineering Structures*, 140, 14–25, 2017.

[17] Walport F., Gardner L. and Nethercot D.A. Design of structural stainless steel members by second order inelastic analysis with CSM strain limits. Submitted to *Thin-Walled Structures*, 2020.

[18] Steel Construction Institute (SCI). Design Manual for Structural Stainless Steel. 4th Edition, 2017.

[19] Gardner L., Fieber A. and Macorini L. Formulae for calculating elastic local buckling stresses of full structural cross-sections. *Structures* 17, 2–20, 2019.

[20] Li Z. and Schafer B.W. Buckling analysis of cold-formed steel members with general boundary conditions using CUFSM: conventional and constrained finite strip methods. Twentieth International Speciality Conference on Cold-Formed Steel Structures. Saint Louis, Missouri, USA, 2010.

[21] prEN 1993-1-1. Eurocode 3 – Design of Steel Structures – Part 1-1: General rules and rules for buildings. Final Document; 2019.

[22] Arrayago I. and Real E. Experimental study on ferritic stainless steel RHS and SHS cross-sectional resistance under combined loading. *Structures*, 4, 69–79, 2015.

[23] Zhao O., Rossi B., Gardner L. and Young B. Behaviour of structural stainless steel cross-sections under combined loading – Part II: Numerical modelling and design approach. *Engineering Structures*, 89, 247–259, 2015.

[24] Kucukler M., Gardner L. and Bu Y. Flexural-torsional buckling of stainless steel I-section beam-columns: Testing, numerical modelling and design. *Thin-Walled Structures* (in press).

[25] Talja A. and Salmi P. Design of stainless steel RHS beams, columns and beam columns. Research note 1619, VTT building technology, Finland, 1995.

[26] Gardner L. and Nethercot D. A. Experiments on stainless steel hollow sections – Part 2: Member behaviour of columns and beams. *Journal of Constructional Steel Research*, 60(9), 1319–1332, 2004.

[27] Liu Y. and Young B. Buckling of stainless steel square hollow section compression members. *Journal of Constructional Steel Research*, 59(2), 165–177, 2003.

[28] Young B. and Liu Y. Experimental investigation of cold-formed stainless steel columns. *Journal of Structural Engineering (ASCE)*, 129(2), 169–176, 2003.

[29] Gardner L., Talja A. and Baddoo N.R. Structural design of high-strength austenitic stainless steel. *Thin-Walled Structures*, 44(5), 517–528, 2006.

[30] Rasmussen K.J.R. and Hancock, G.J. Design of cold-formed stainless steel tubular members. I: Columns. *Journal of Structural Engineering (ASCE)*, 119(8), 2349–2367, 1993.

[31] Afshan S. and Gardner L. Experimental study of cold-formed ferritic stainless steel hollow sections. *Journal of Structural Engineering (ASCE)*, 139(5), 717–728, 2013.

[32] Zhao O., Gardner L. and Young B. Buckling of ferritic stainless steel members under combined axial compression and bending. *Journal of Constructional Steel Research*, 117, 35–48, 2016.

[33] Theofanous M. and Gardner L. Testing and numerical modelling of lean duplex stainless steel hollow section columns. *Engineering Structures*, 31(12), 3047–3058, 2009.

[34] Huang Y. and Young B. Tests of pin-ended cold-formed lean duplex stainless steel columns. *Journal of Constructional Steel Research*, 82, 203–215, 2013.

[35] Young B. and Lui W. M. Tests on cold formed high strength stainless steel compression members. *Thin-Walled Structures*, 44(2), 224–234, 2006.

[36] Lui W.M., Ashraf M. and Young B. Tests of cold-formed duplex stainless steel SHS beam-columns. *Engineering Structures*, 74, 111–121, 2014.

[37] ABAQUS. ABAQUS/Standard user's manual volumes I-III and ABAQUS CAE manual. Dassault Systemes Simulia Corporation, 2014.

[38] Li H.T and Young B. Web crippling of cold-formed ferritic stainless steel square and rectangular hollow sections. *Engineering Structures*, 176, 968–980, 2018.

[39] Arrayago I., Picci F., Mirambell E. and Real E. Interaction of bending and axial load for ferritic stainless steel RHS columns. *Thin-Walled Structures*, 91, Pages 96–107, 2015.

[40] Cruise R.B. and Gardner L. Strength enhancements induced during cold forming of stainless steel sections. *Journal of Constructional Steel Research*, 64(11), 1310–1316, 2008.

[41] Jandera M., Gardner L. and Machacek J. Residual stresses in cold-rolled stainless steel hollow sections. *Journal of Constructional Steel Research*, 64 (11), 1255–1263, 2008.

[42] Gardner L. and Cruise R.B. Modeling of residual stresses in structural stainless steel sections. *Journal of Structural Engineering (ASCE)*, 135(1), 42–53, 2009.

[43] Dawson R.G. and Walker A.C. Post-buckling of geometrically imperfect plates. *Journal of the Structural Division (ASCE)*, 98(1), 75–94, 1972.

[44] Gardner L. and Nethercot D.A. Numerical modeling of stainless steel structural components – A consistent approach. *Journal of Structural Engineering (ASCE)*, 130(10), 1586–1601, 2004.

[45] Arrayago I., Real E. and Gardner L. Description of stress–strain curves for stainless steel alloys. *Materials & Design*, 87, 540–552, 2015.

[46] Maquoi R. and Rondal J. Mise en équation des nouvelles courbes Européennes de flambement, *Construction Métallique*, 1, 17–30, 1978.

[47] Afshan S., Zhao O. and Gardner L. Standardised material properties for numerical parametric studies of stainless steel structures and buckling curves for tubular columns. *Journal of Constructional Steel Research*, 152, 2–11, 2019.

[48] European Committee for Standardization. EN 1990. European Committee for Standardization Eurocode. Basis of structural design. Brussels, Belgium, 2005.

[49] Trahair N.S., Bradford M.A., Nethercot D.A. and Gardner L. The Behaviour and Design of Steel Structures to EC3. Fourth edition. 2008.

[50] Simoes da Silva L., Simoes R. and Gervasio H. Design of Steel Structures. Eurocode 3: Design of steel structures – Part 1-1: General rules – General rules and rules for buildings. ECCS Eurocode Design Manuals. First edition. 2010.

[51] Gardner L. Stability and design of stainless steel structures – Review and outlook. *Thin-Walled Structures*, 141, 208–216, 2019.

[52] Walport F., Gardner L. and Nethercot, D.A. Equivalent bow imperfections for design by second order inelastic analysis. Submitted to *Structures*, 2020.

[53] Gardner L. and Theofanous M. Discrete and continuous treatment of local buckling in stainless steel elements. *Journal of Constructional Steel Research*, 64, 1207–1216, 2008.

[54] Afshan S., Francis P., Baddoo N.R. and Gardner L. Reliability analysis of structural stainless steel design provisions. *Journal of Constructional Steel Research*, 114, 293–304, 2015.

[55] Bu Y. and Gardner L. Laser-welded stainless steel I-section beam-columns: Testing, simulation and design. *Engineering Structures*, 179, 23–36, 2019.

[56] Meng X., Gardner L., Sadowski A.J. and Rotter J.M. Elasto-plastic behaviour and design of semi-compact circular hollow sections. *Thin-Walled Structures* 148, 106486, 2020.

FIGURES

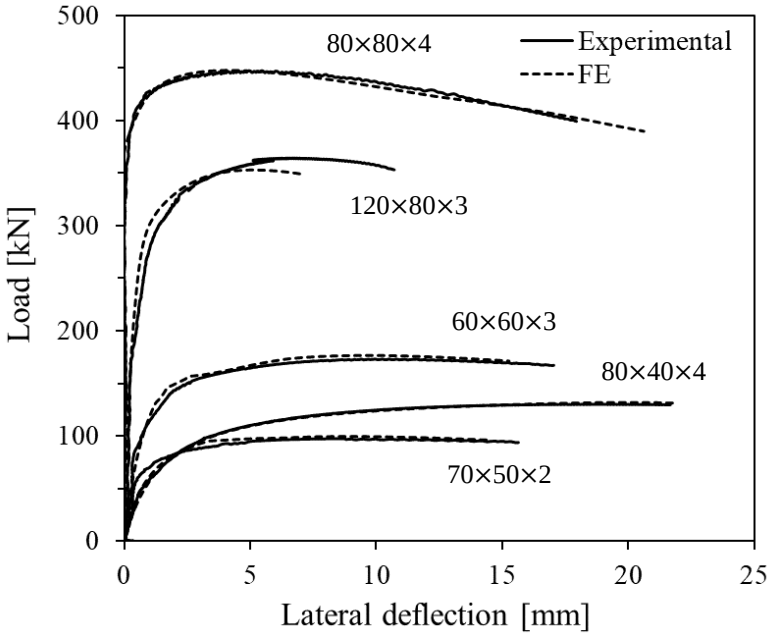

Figure 1. Comparison of experimental and FE load-lateral deflection curves for ferritic stainless steel columns.

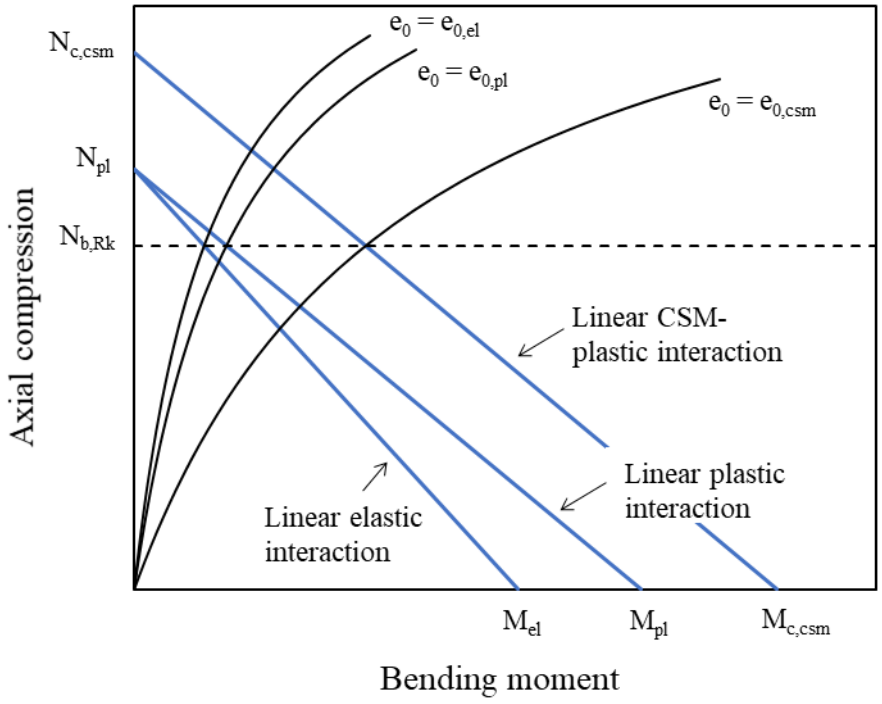

Figure 2. Critical cross-section N-M equilibrium paths obtained using GNIA with back-calculated equivalent bow imperfection amplitudes e_0 and different linear interaction equations.

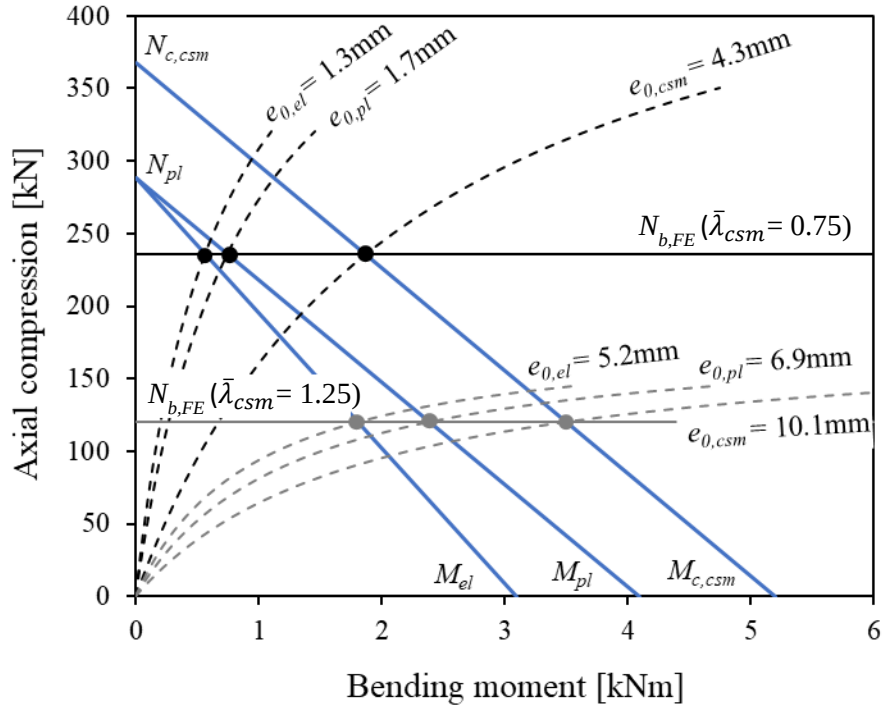

Figure 3. N-M interaction diagrams and determination of flexural buckling resistance for austenitic stainless steel columns with $\bar{\lambda}_{csm} = 0.75$ and $\bar{\lambda}_{csm} = 1.25$.

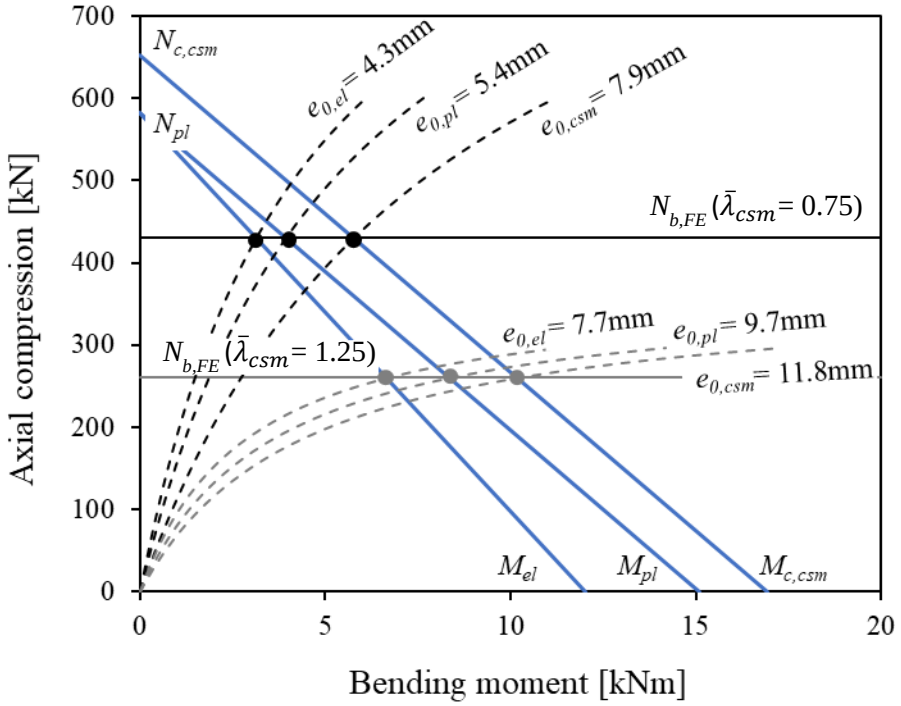

Figure 4. N-M interaction diagrams and determination of flexural buckling resistance for ferritic stainless steel columns with $\bar{\lambda}_{csm} = 0.75$ and $\bar{\lambda}_{csm} = 1.25$.

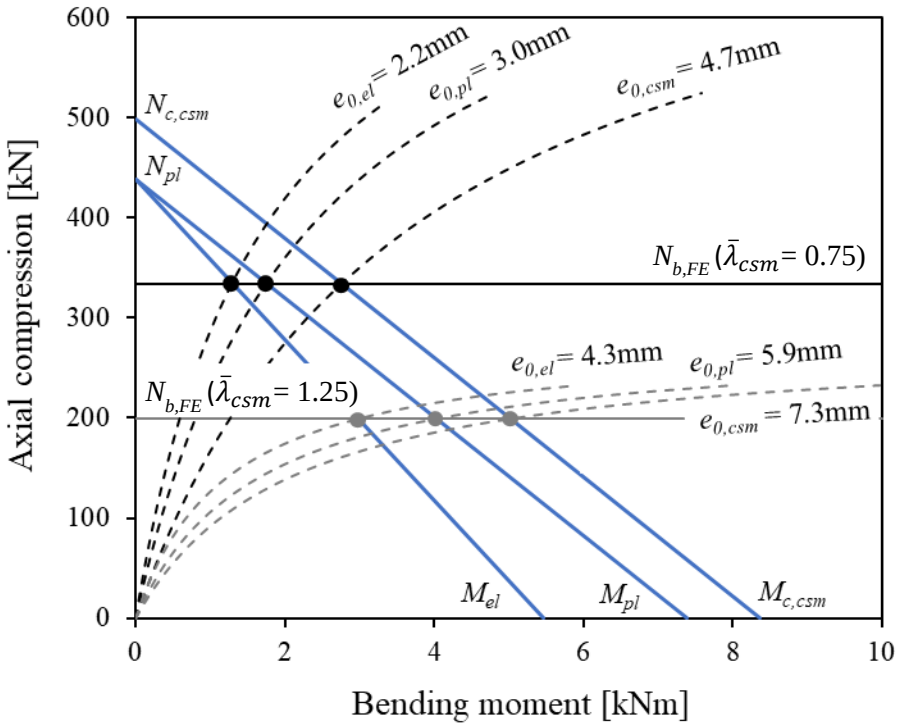

Figure 5. N-M interaction diagrams and determination of flexural buckling resistance for duplex stainless steel columns with $\bar{\lambda}_{csm} = 0.75$ and $\bar{\lambda}_{csm} = 1.25$.

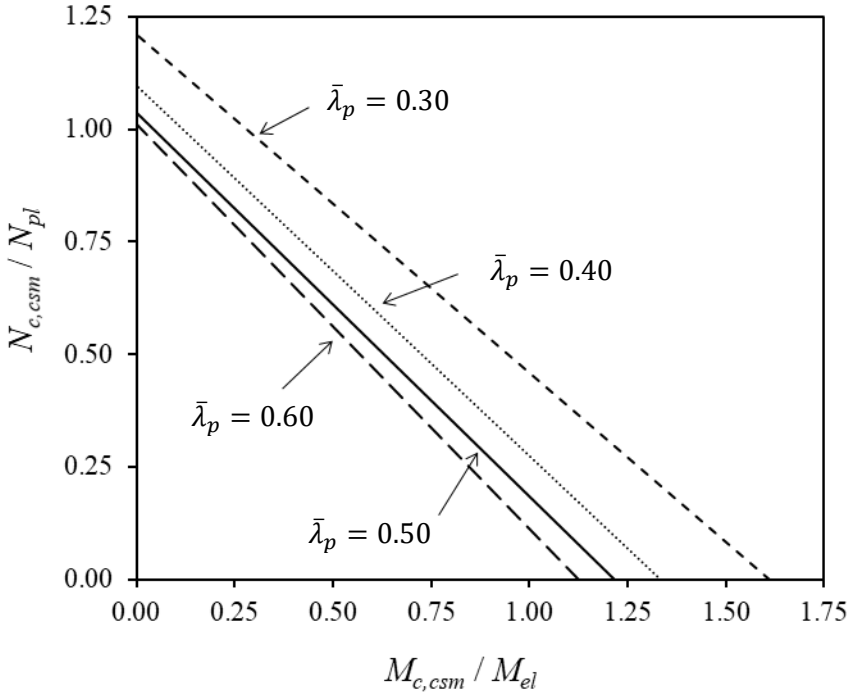

Figure 6. Influence of the cross-section slenderness in linear CSM-plastic interaction diagrams.

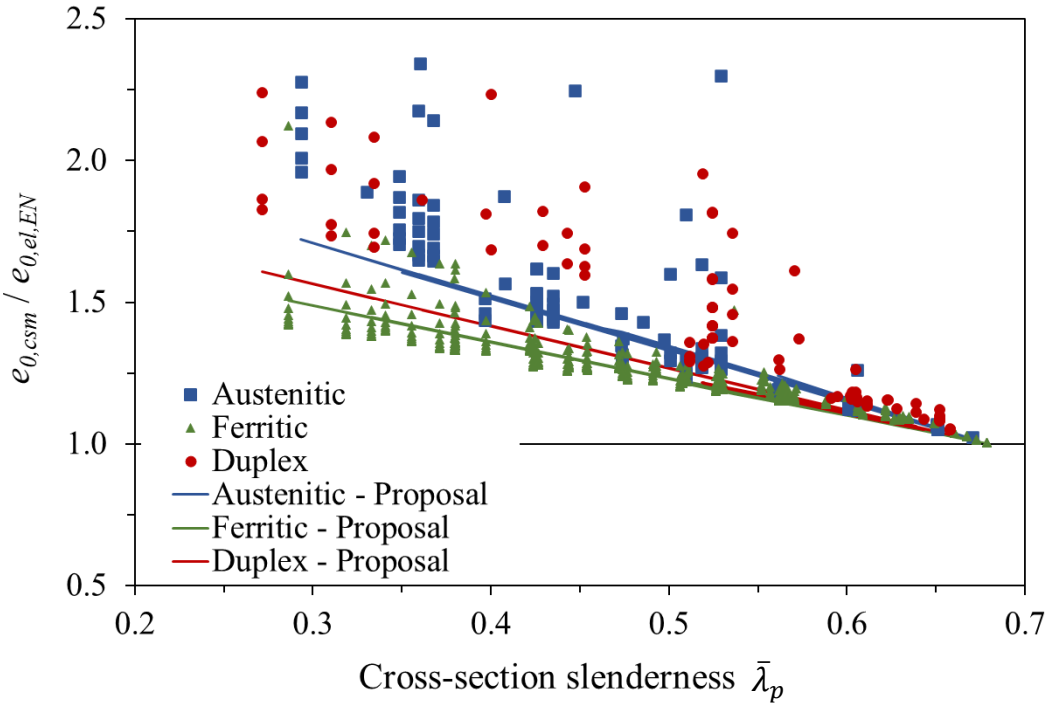

Figure 7. Relationship between CSM and EN equivalent bow imperfection amplitudes as a function of local slenderness $\bar{\lambda}_p$.

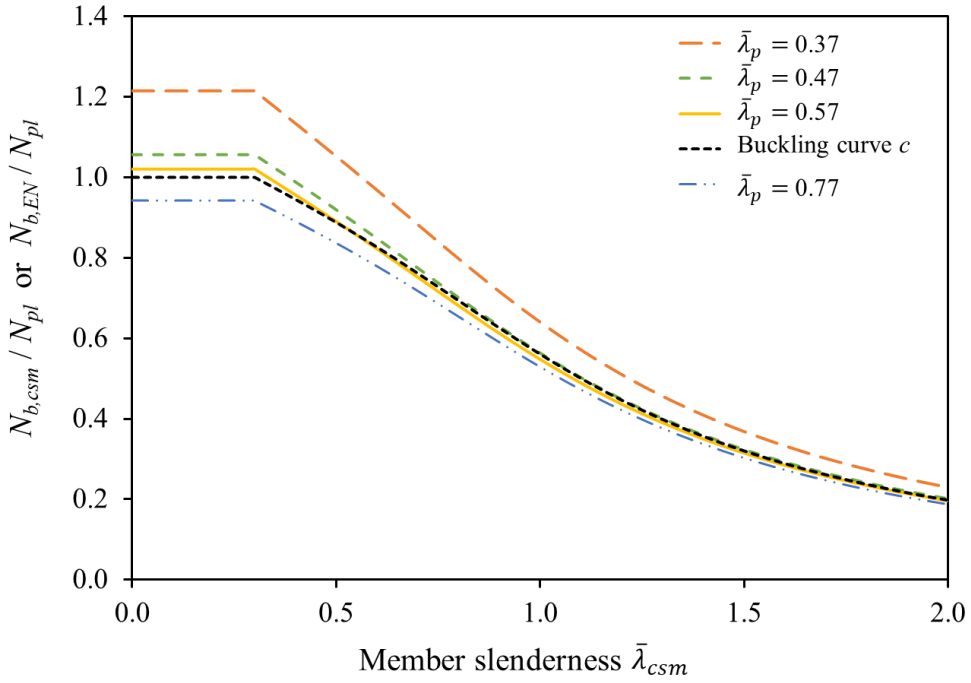

Figure 8. CSM member buckling curves for austenitic stainless steel SHS/RHS columns.

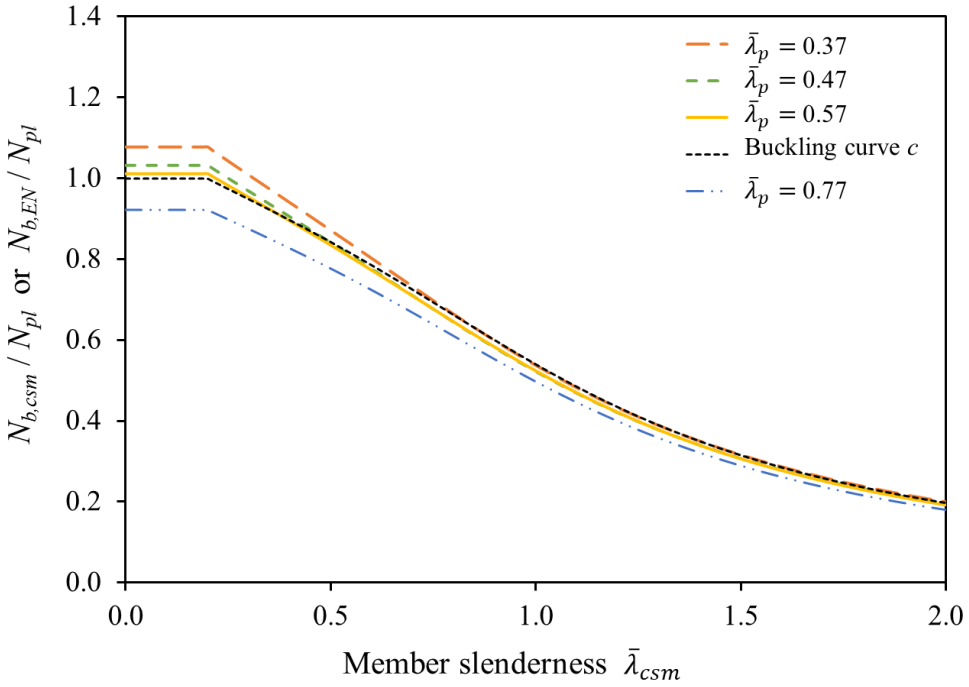

Figure 9. CSM member buckling curves for ferritic stainless steel SHS/RHS columns.

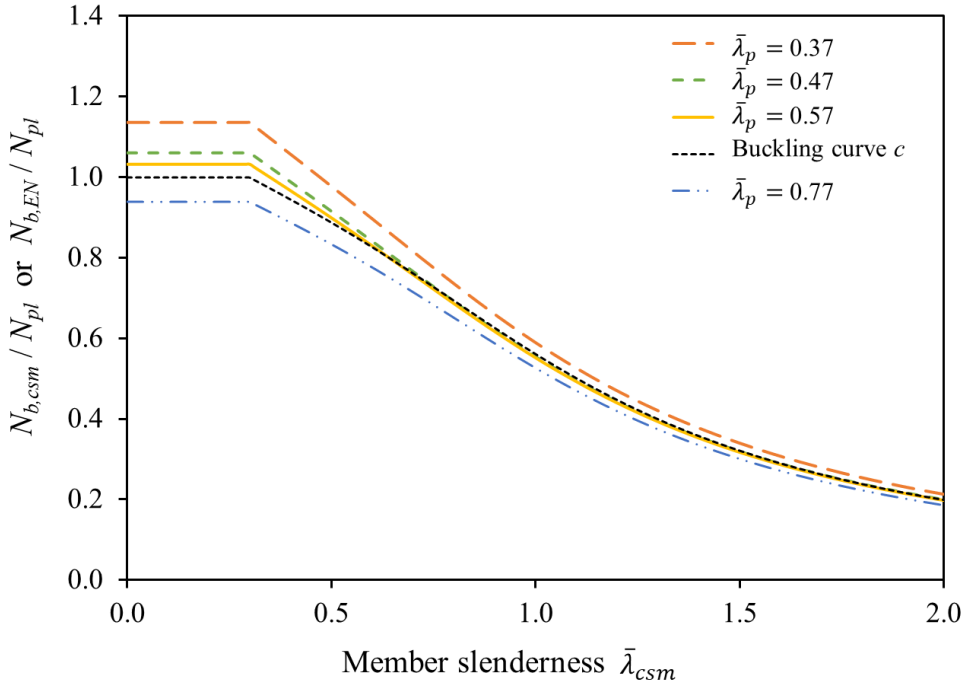

Figure 10. CSM member buckling curves for duplex stainless steel SHS/RHS columns.

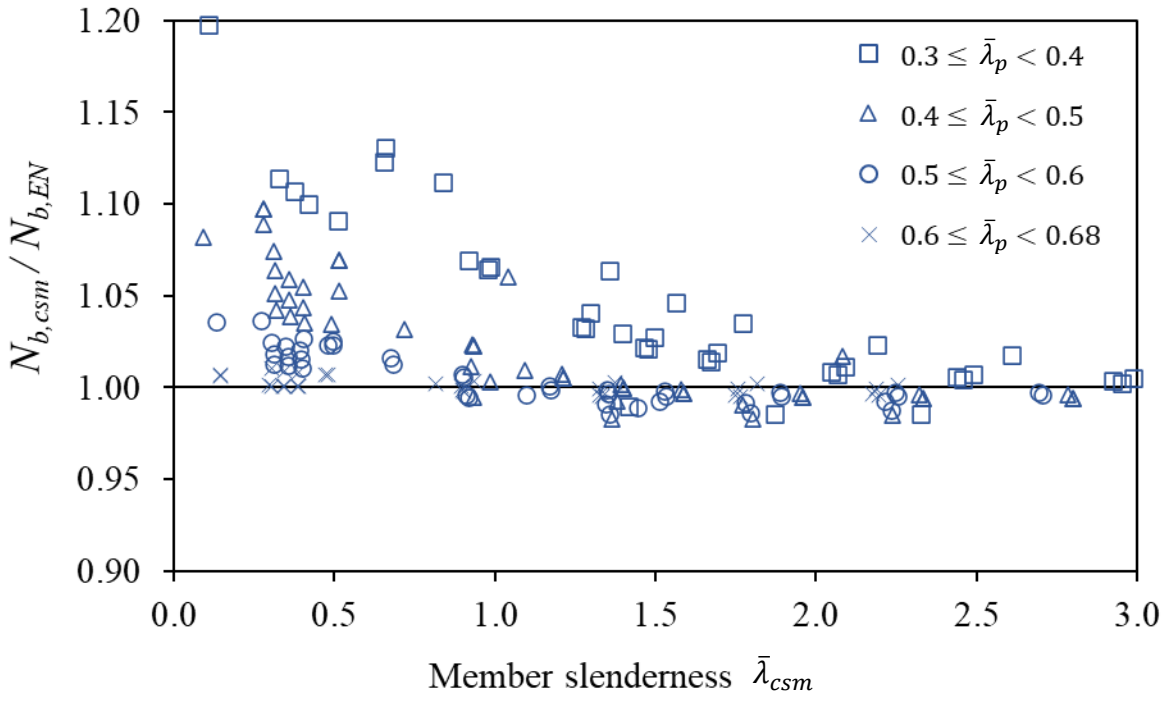

Figure 11. Comparison between buckling resistance predictions obtained using the proposed CSM member design approach and EN 1993-1-4 [1] for austenitic stainless steel SHS/RHS columns.

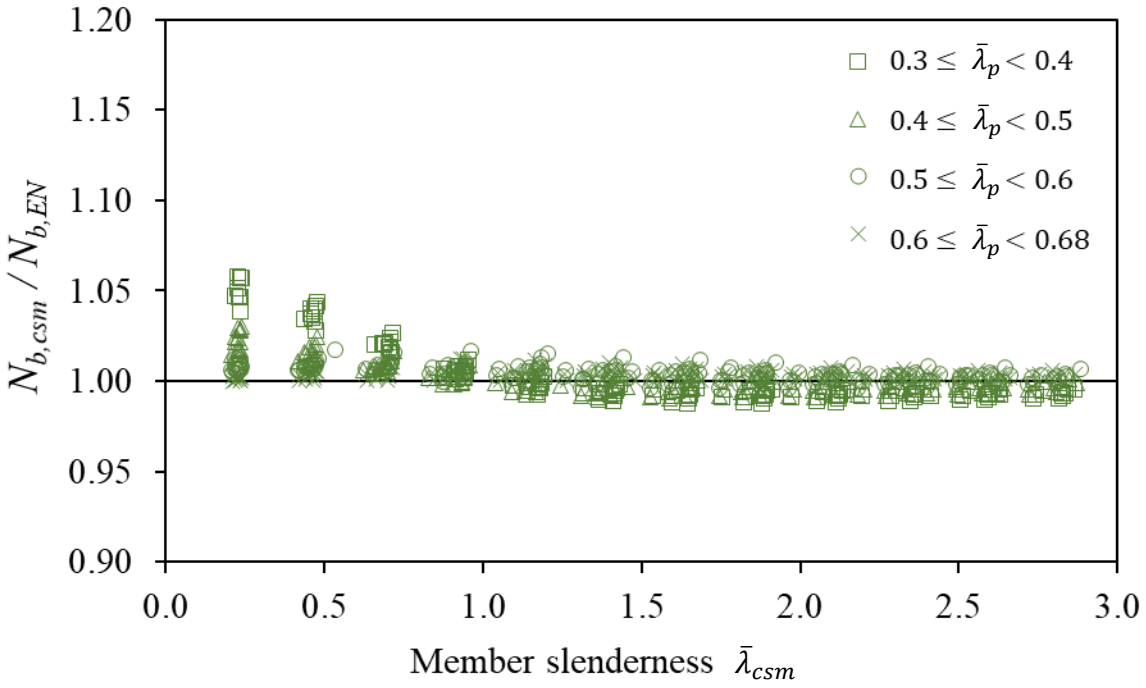

Figure 12. Comparison between buckling resistance predictions obtained using the proposed CSM member design approach and EN 1993-1-4 [1] for ferritic stainless steel SHS/RHS columns.

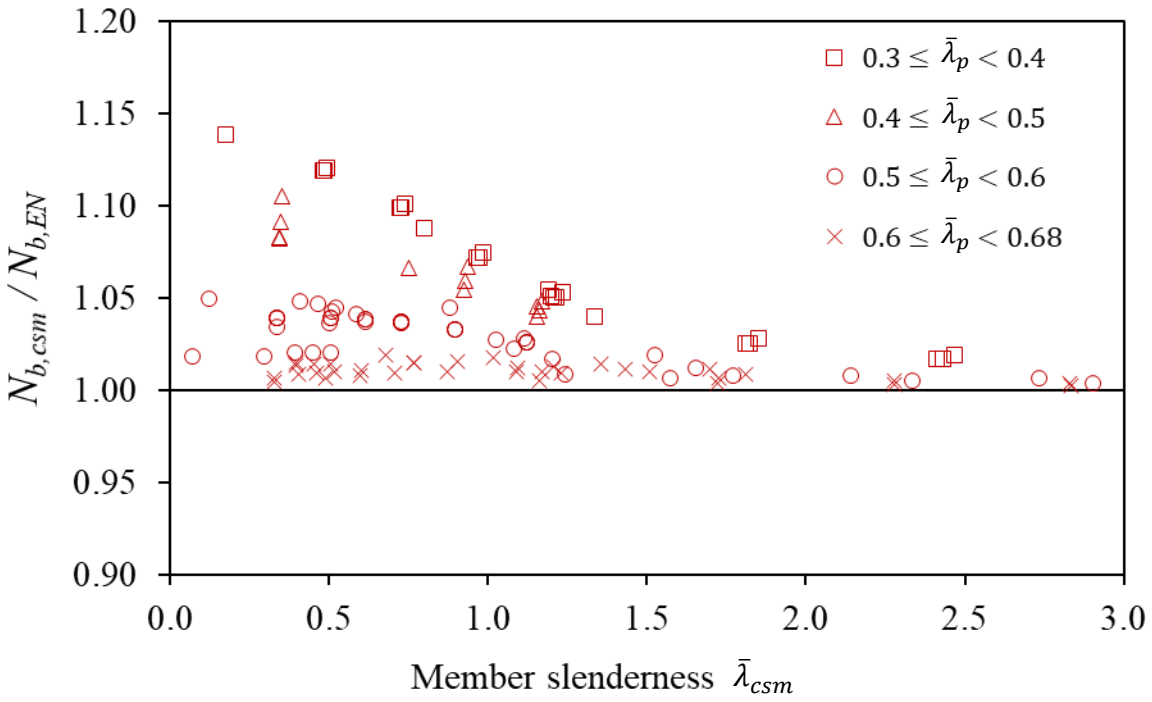

Figure 13. Comparison between buckling resistance predictions obtained using the proposed CSM member design approach and EN 1993-1-4 [1] for duplex stainless steel SHS/RHS columns.

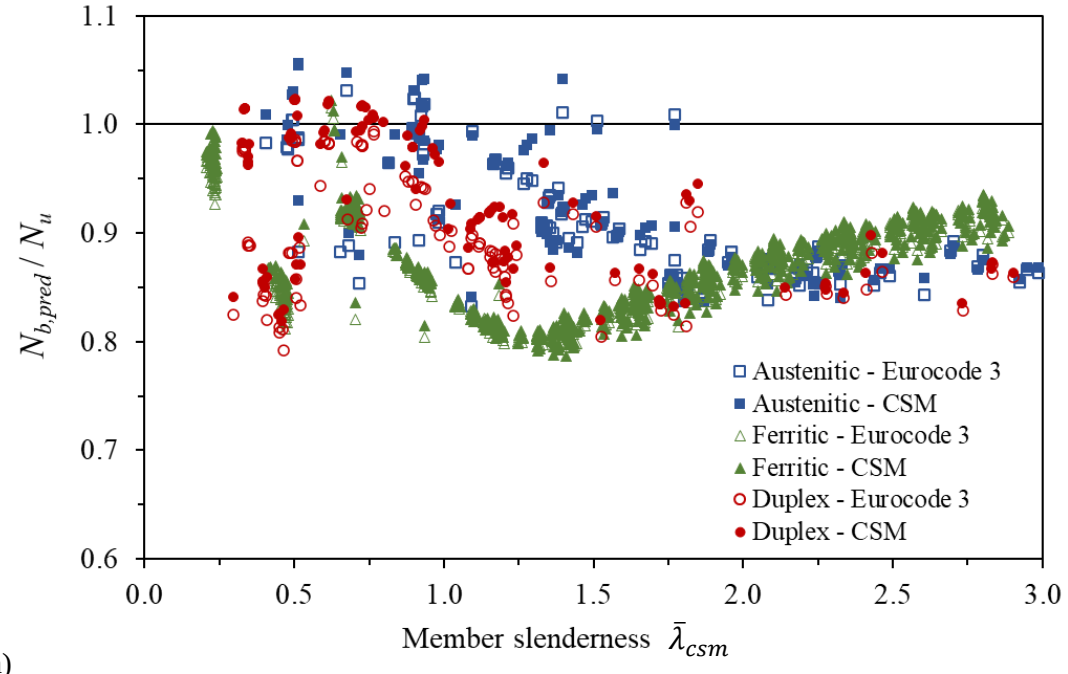

(a)

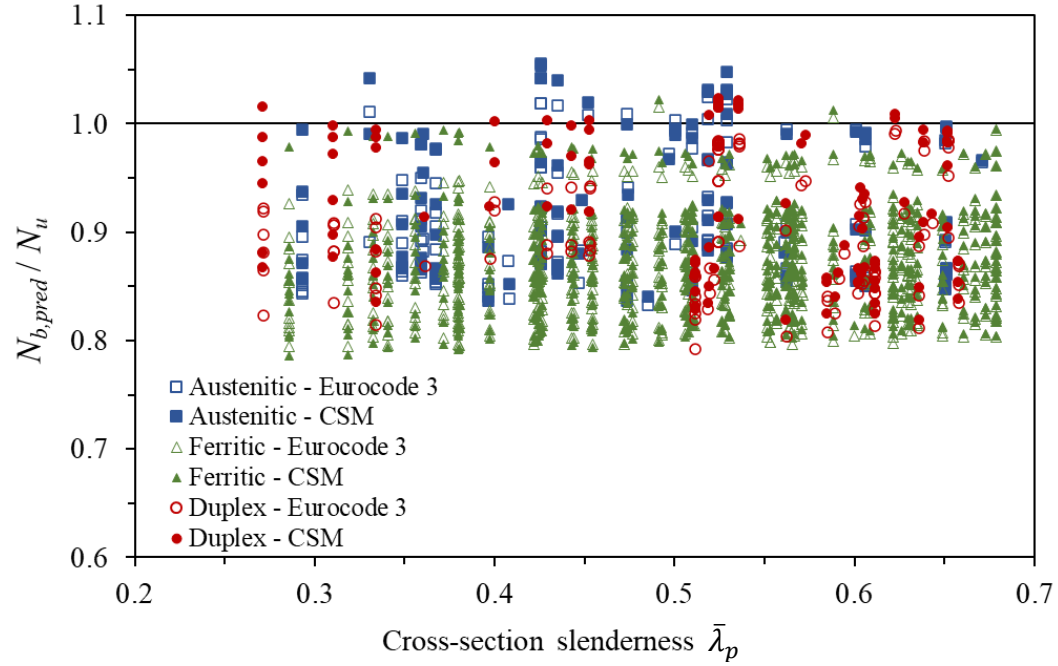

(b)

Figure 14. Assessment of the proposed CSM and Eurocode 3 [18,47] approaches for stainless steel SHS/RHS columns with stocky cross-sections ($\bar{\lambda}_p \leq 0.68$).

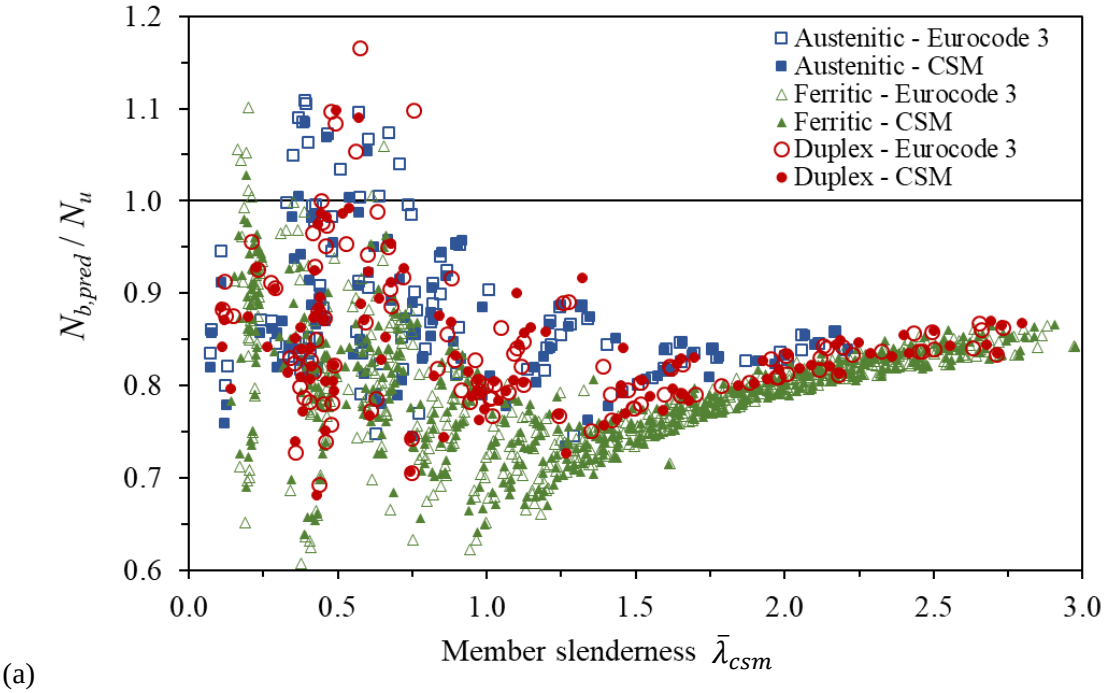

(a)

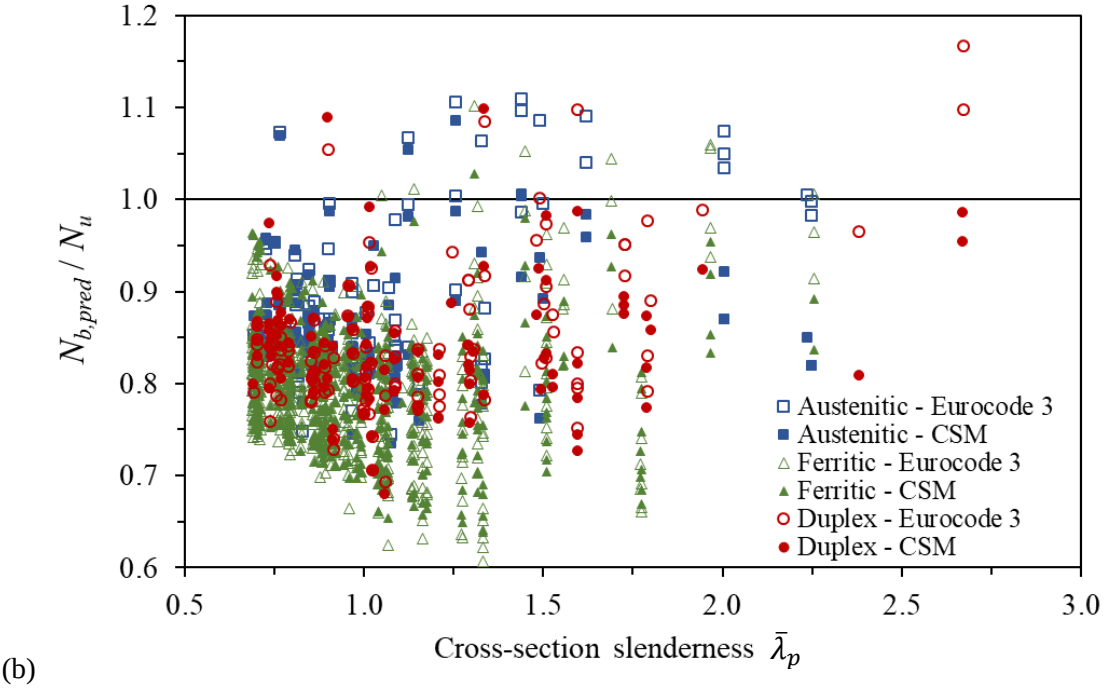

(b)

Figure 15. Assessment of the proposed CSM and Eurocode 3 [18,47] approaches for stainless steel SHS/RHS columns with slender cross-sections ($\bar{\lambda}_p > 0.68$).

TABLES

Table 1. CSM material model coefficients.

Stainless steel type	C_1	C_2	C_3
Austenitic	0.10	0.16	1.00
Ferritic	0.40	0.45	0.60
Duplex	0.10	0.16	1.00

Table 2. Summary of assembled experimental data on stainless steel tubular section columns.

Stainless steel type	Material grade	No. of tests	Boundary conditions	Range of cross-section slenderness $\bar{\lambda}_p$	Range of member slenderness $\bar{\lambda}$	Reference
Austenitic	1.4301	12	Pin-ended	0.27-0.98	0.52-1.92	[25]
	1.4301	22	Pin-ended	0.28-1.17	0.39-1.95	[26]
	1.4301	12	Fixed-ended	0.27-0.71	0.27-1.07	[27]
	1.4301	24	Fixed-ended	0.39-1.26	0.30-1.72	[28]
	1.4318	12	Pin-ended	0.59-0.86	0.59-1.66	[29]
	1.4307	4	Pin-ended	0.50-0.52	0.14-1.43	[30]
Ferritic	1.4003	5	Pin-ended	0.46-0.94	0.69-1.76	[6]
	1.4003	11	Pin-ended	0.41-0.91	0.31-2.43	[31]
	1.4509	4	Pin-ended	0.55	0.80-1.74	[31]
	1.4003	2	Pin-ended	0.54-0.56	0.43-1.21	[32]
Duplex	1.4162	12	Pin-ended	0.49-0.54	0.58-2.07	[33]
	1.4162	43	Pin-ended	0.50-1.73	0.20-2.67	[34]
	-	20	Fixed-ended	0.51-1.32	0.28-1.80	[35]
	1.4462	5	Pin-ended	0.49-0.84	0.50-1.43	[36]

Table 3. Comparison between experimental and FE results for ferritic stainless steel columns.

Specimen	$N_{u,FE}/N_{u,exp}$	$\delta_{u,FE}/\delta_{u,exp}$
80×80×4	1.00	0.93
60×60×3	1.02	0.99
80×40×4	1.01	1.03
120×80×3	0.97	0.80
70×50×2	1.02	1.00
Mean	1.00	0.95
COV	0.021	0.096

Table 4. Definition of material properties for parametric studies

Stainless steel type	Cross-section region	E [GPa]	f_y [MPa]	f_u [MPa]	ε_u [%]	n	m	Source
Austenitic	Flat	196	355	608	0.45	5.9	3.5	[7]
	Corner	201	559	725	0.28	4.8	4.1	[7]
Ferritic	Flat	187	485	505	0.07	12.2	2.6	[6]
	Corner	178	555	587	0.01	7.9	5.2	[6]
Duplex	Flat	198	635	756	0.44	6.0	4.2	[7]
	Corner	207	833	1079	0.23	5.0	6.1	[7]

Table 5. Assessment of design approaches for stainless steel SHS/RHS members with stocky cross-sections ($\bar{\lambda}_p \leq 0.5$) in compression.

Stainless steel type			Eurocode 3 $N_{b,EN}/N_u$	CSM $N_{b,csm}/N_u$	Eurocode 3 $N_{b,EN}/N_u$	CSM $N_{b,csm}/N_u$
			Stocky members $\bar{\lambda}_{csm} \leq 1$		Slender members $\bar{\lambda}_{csm} > 1$	
Austenitic	Exp.	Mean	0.91	0.95	0.90	0.91
		COV	0.060	0.050	0.084	0.071
	FE	Mean	0.96	1.02	0.89	0.90
		COV	0.056	0.033	0.042	0.052
	All	Mean	0.94	0.99	0.89	0.90
		COV	0.061	0.054	0.046	0.053
Ferritic	Exp.	Mean	-	-	-	-
		COV	-	-	-	-
	FE	Mean	0.89	0.91	0.86	0.85
		COV	0.055	0.060	0.044	0.044
	All	Mean	0.89	0.91	0.86	0.85
		COV	0.055	0.060	0.044	0.044
Duplex	Exp.	Mean	-	-	-	-
		COV	-	-	-	-
	FE	Mean	0.91	0.99	0.87	0.90
		COV	0.024	0.016	0.037	0.037
	All	Mean	0.91	0.99	0.87	0.90
		COV	0.024	0.016	0.037	0.037

Table 6. Assessment of design approaches for stainless steel SHS/RHS members in compression for the full cross-section slenderness range.

Stainless steel type			Eurocode 3 $N_{b,EN}/N_u$	CSM $N_{b,csm}/N_u$
Austenitic	Exp.	Mean	0.91	0.93
		COV	0.070	0.064
	FE	Mean	0.89	0.90
		COV	0.074	0.075
	All	Mean	0.89	0.90
		COV	0.074	0.075
Ferritic	Exp.	Mean	0.84	0.85
		COV	0.047	0.051
	FE	Mean	0.87	0.87
		COV	0.052	0.055
	All	Mean	0.87	0.87
		COV	0.052	0.055
Duplex	Exp.	Mean	0.89	0.90
		COV	0.062	0.065
	FE	Mean	0.89	0.93
		COV	0.061	0.070
	All	Mean	0.90	0.93
		COV	0.062	0.072

Table 7. Assessment of design approaches for stainless steel SHS/RHS members with slender cross-sections ($\bar{\lambda}_p > 0.68$) in compression

Stainless steel type			Eurocode 3 $N_{b,EN}/N_u$	CSM $N_{b,csm}/N_u$
Austenitic	Exp.	Mean	0.84	0.83
		COV	0.056	0.060
	FE	Mean	0.92	0.88
		COV	0.101	0.080
	All	Mean	0.89	0.87
		COV	0.099	0.079
Ferritic	Exp.	Mean	0.82	0.82
		COV	0.047	0.056
	FE	Mean	0.80	0.79
		COV	0.089	0.078
	All	Mean	0.79	0.79
		COV	0.096	0.078
Duplex	Exp.	Mean	0.85	0.84
		COV	0.079	0.067
	FE	Mean	0.85	0.84
		COV	0.102	0.085
	All	Mean	0.85	0.84
		COV	0.096	0.081

Table 8. Summary of the reliability analysis results for the CSM and Eurocode 3 approaches for stainless steel SHS/RHS members in compression.

	Design approach	Stainless steel type	b	V_δ	V_r	γ_{M1}
Stocky cross-sections	Eurocode 3	Austenitic	1.131	0.076	0.109	1.01
		Ferritic	1.152	0.052	0.085	0.98
		Duplex	1.119	0.062	0.085	0.98
$\bar{\lambda}_p \leq 0.68$ $\bar{\lambda}_{csm} \in [0.23,2.98]$	CSM	Austenitic	1.113	0.076	0.109	1.03
		Ferritic	1.148	0.054	0.087	0.99
		Duplex	1.084	0.071	0.092	1.05
Slender cross-sections	Eurocode 3	Austenitic	1.135	0.092	0.121	1.07
		Ferritic	1.259	0.086	0.110	1.05
		Duplex	1.187	0.092	0.109	1.09
$\bar{\lambda}_p > 0.68$ $\bar{\lambda}_{csm} \in [0.11,2.98]$	CSM	Austenitic	1.156	0.076	0.109	1.02
		Ferritic	1.258	0.079	0.104	1.03
		Duplex	1.186	0.088	0.106	1.08